Journal of Fluorine Chemistry 131 (2010) 495–504

Contents lists available at ScienceDirect

Journal of Fluorine Chemistry

journal homepage: www.elsevier.com/locate/fluor

Chirality-dependent sublimation of α-(trifluoromethyl)-lactic acid: Relative vapor pressures of racemic, eutectic, and enantiomerically pure forms, and vibrational spectroscopy of isolated (*S*,*S*) and (*S*,*R*) dimers

Merwe Albrecht [a], Vadim A. Soloshonok [b,c], Lena Schrader [a], Manabu Yasumoto [d], Martin A. Suhm [a,*]

[a] *Institut für Physikalische Chemie, Universität Göttingen, Tammannstr. 6, D-37077 Göttingen, Germany*
[b] *Department of Chemistry and Biochemistry, The University of Oklahoma, Norman, OK 73019-3051, USA*
[c] *Institute of Bioorganic Chemistry and Petrochemistry, National Academy of Sciences of the Ukraine, Murmanska Street, Kyiv-94 02660, Ukraine*
[d] *Central Glass Co., 2805 Imafuku-nakadai Kawagoe-shi, Saitama 350-1151, Japan*

ARTICLE INFO

Article history:
Received 1 October 2009
Received in revised form 16 November 2009
Accepted 18 November 2009
Available online 24 November 2009

Keywords:
Eutectic
Sublimation
Chirality
Dimer
Racemate
Infrared

ABSTRACT

A mass-spectrometric determination of the sublimation pressure diagram of α-(trifluoromethyl)-lactic acid as a function of its enantiomeric composition at 293 K shows that the racemic crystals have a 38 ± 15% higher volatility than the enantiomerically pure crystals and the sublimation eutectic has a 55 ± 10% higher vapor pressure. These data indicate a possibility for thermodynamically controlled enantiomeric enrichment of the residual material via sublimation of samples of higher than 35 ± 10% ee. The vibrational spectroscopy of isolated (*S*,*S*) and (*S*,*R*) dimers in supersonic jets shows that chirality recognition effects are restricted to larger clusters. This is a consequence of the rigid planar carboxylic acid binding motif.

1. Introduction

Chiral enantiomerically enriched compounds can change their enantiomeric composition under otherwise achiral conditions in a range of ways [1,2]. One of them, fractional crystallization, is a well-established, routine procedure for optical purification of the excess enantiomer [3–5]. It usually profits from an enhanced stability of the solid racemic compound over the enantiomerically pure crystals [4]. On the other hand, other physical processes which can lead to similar chiroptical outcomes, such as achiral-phase chromatography [6–8], sublimation [9–14], gravitational field [15,16] and even distillation [17–19], remain less studied. The general phenomenon, separation of racemate from the excess enantiomer under otherwise achiral conditions, has been denoted self-disproportionation of enantiomers (SDE) [7].

Sublimation is a particularly intriguing approach because it shows large effects, does not require auxiliary compounds, and works better for less stable racemic compounds. Actually, it becomes rather trivial if the racemic compound is not stable at all and a conglomerate of (*R*) and (*S*) crystals forms, instead. In this case, the enantiomers can sublimate independent of each other and ideally, any small excess will persist in the residue, increasing its ee-value up to 100%. In practice, crystal size and packing may lead to deviations, unless the sublimation process occurs under thermodynamic equilibrium conditions. The latter are therefore particularly desirable for a fundamental study, although practical procedures will usually involve kinetic control.

Conglomerate formation is rare. More frequently, one or more crystalline compounds with stoichiometric composition (R_nS_m) will form and may differ in their vapor pressure from the pure (*R*) and (*S*) forms. In favorable cases, these mixed solids (congruently sublimating or dystectic points in the phase diagram) have a higher vapor pressure than the enantiomerically pure compound and may thus still carry away efficiently the unwanted enantiomer upon sublimation. This requires that the sample is sufficiently enantiomerically pure from the start, as we will see. A further constraint is that for a given temperature, the equilibrium vapor pressure of any solid mixture of enantiomers cannot exceed twice that of the enantiomerically pure solid, because otherwise it would be unstable with respect to a conglomerate.

The advantages of sublimation in terms of conceptual simplicity and solvent-free operation must be balanced against some restrictions. The most obvious one is a limit in the applicable temperature range which must be below the melting point of a

* Corresponding author.
E-mail address: msuhm@gwdg.de (M.A. Suhm).

0022-1139/$ – see front matter © 2009 Elsevier B.V. All rights reserved.
doi:10.1016/j.jfluchem.2009.11.015

given compound, where vapor pressures are typically low and difficult to measure. Measurements at room temperature or below are particularly challenging, because not many chiral compounds exhibit sufficient volatility. Therefore, the analogous properties of solution phase diagrams are usually exploited [20], but the charm of modeling a single compound (and its mirror image) in the two simplest states of aggregation is lost.

An exceptional case of solid state volatility and vapor pressure differences was recently reported for α-(trifluoromethyl)-lactic acid [14]. Here, the racemate vapor pressure at somewhat elevated temperatures exceeds that of the enantiomerically pure crystals by as much as 50%, half way to the thermodynamic limit. The reasons for such an exceptional difference can be traced back to differences in intermolecular interaction. These may be located in the solid state [21] or – much less likely [20] – in the gas phase. If the gas phase shows enantioselective aggregation [22], it is in principle conceivable that this contributes to the phenomenon. As carboxylic acids are well known for their gas phase dimerization propensity [23], it is worth exploring the gas phase in some detail in this particular case. More importantly, gas phase aggregation provides a universal stepwise approach towards solid state aggregation, well suitable for theoretical modeling. For this reason, we have initiated a gas phase aggregation study of α-(trifluoromethyl)-lactic acid (TFMLA), using supersonic jet cooling for an accurate characterization of the vibrational dynamics in its dimers. We use IR spectroscopy, because microwave spectroscopy would not be able to detect inversion-symmetric (*R*/*S*) dimers [24]. We use FTIR spectroscopy, because TFMLA does not have a suitable UV chromophore for double resonance studies [25] and a direct absorption approach is thus needed. The experimental results are supported by quantum chemical calculations for the monomer and the dimer of TFMLA. Furthermore, we explore the sublimation phase diagram of TFMLA at ambient temperature for the first time, using a simple mass spectrometry setup for the detection of TFMLA partial pressures.

2. Materials and methods

2.1. Procedure for the synthesis of TFMLA

The enantiomerically pure (*S*), **1** and racemic (*S*/*R*), **2** forms of TFMLA were synthesized according to the large-scale procedures developed by some of us, which are described in the following part in full detail. Two different batches of compound were used in our investigations. Furthermore, a commercial sample of the racemate (TCI Europe, >98%) was used without further purification. No spectral difference between the commercial and the synthesized samples was observed.

Preparation of **4**:

To the solution of compound **3** in THF (100 g, 0.46 mol), methylmagnesium chloride (commercial 3M in THF, 186 mL, 0.56 mol) was added under stirring drop wise keeping the temperature under 0 °C. After the addition was completed, the resulting mixture was stirred for 1 h at −20 °C, and the solution followed by addition of 10% HCl (200 mL). The organic layer was separated from the aqueous phase and distilled to obtain **4** as a 75 wt% THF solution (126.1 g, 0.41 mol, calculated yield 89%).

Preparation of **5**:

To the solution of KOMe in methanol (32% in methanol, 358.5 g, 1.64 mol), compound **4** (75 wt% THF solution, 126.1 g, 0.41 mol) was added under stirring drop wise, keeping the temperature 40–45 °C. After addition was complete, the mixture was stirred for 12 h at 40 °C. The solution was cooled down to room temperature, and the formed solid was removed by filtration. The mother liquid was distilled to obtain methyl ester **5** (23.6 g, 0.13 mol, yield 31%).

Preparation of **2**:

The mixture of compound **5** (10 g, 0.054 mol) and 48% aq. HBr (72.5 g, 0.43 mol) was heated at 115 ° C for 24 h. After cooling down the reaction mixture to room temperature, the aqueous solution of NaOH (48%, 22.5 g, 0.27 mol) was added to neutralize the HBr. The solution was extracted with ethyl acetate (50 mL ×2), and the combined organic layers were washed with aqueous NaCl (10 wt%, 50 mL). The ethyl acetate was removed under reduced pressure to give the target racemate **2** (7.6 g, 0.048 mol, yield 89%).

Preparation of **6**:

To the solution of methylmagnesium chloride (3M in THF, 39.4 mL, 0.12 mol), (*R*)-(phenyl)ethylamine (13.7 g, 0.11 mol) was added under stirring drop wise, keeping the temperature under 15 °C. After addition was complete, the solution was stirred for 2 h at 5 °C. To the resulting mixture, solution of compound **5** (10 g, 0.054 mol) in THF was added drop wise keeping the temperature under 15 °C. After addition was complete, the resulting solution was stirred for 24 h at room temperature. The mixture was quenched by aqueous HCl (10 wt%, 100 mL), and extracted with ethyl acetate (100 mL ×2). The combined organic layer was washed with aqueous HCl (10 wt%, 100 mL), followed by washing with NaCl (10 wt%, 100 mL). The solvent was removed under reduced pressure to give amide **6** (14.0 g, 0.051 mol, yield 95%).

Optical resolution of **6**:

Thus obtained compound **6** (14.0 g, 0.051 mol) was re-crystallized from a mixture of toluene (7 mL) with n-heptane (84 mL) to give 92% de of compound **7** (6.7 g) containing (*S*) configurated carbon in the acid moiety. Repeating re-crystallization (total three times) under the same conditions gave compound **7** of >99% de (4.8 g, 0.017 mol, yield 34%).

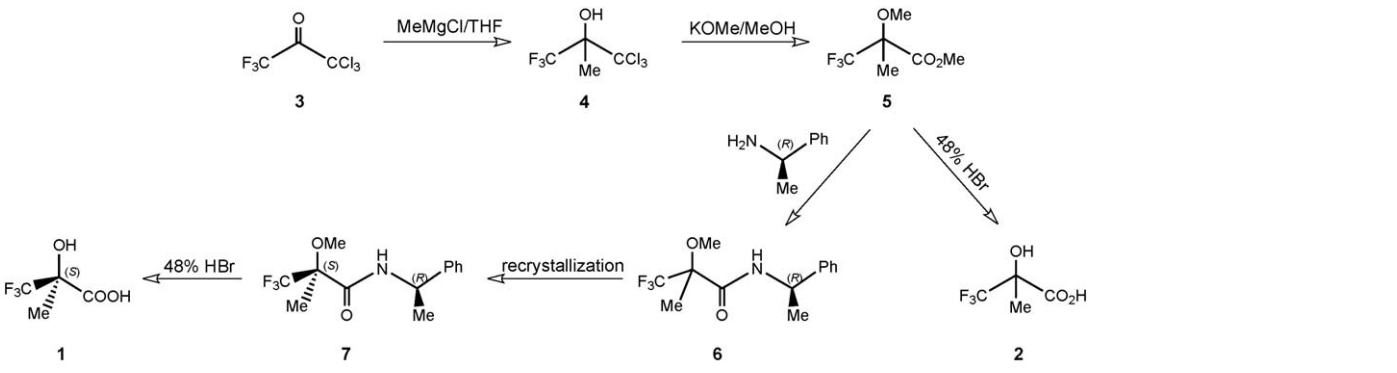

Preparation of **1**:

The mixture of compound **7** (>99% de, 4.8 g, 0.017 mol) and 48% aqueous HBr (22.9 g, 0.14 mol) was heated at 115 °C for 24 h. After cooling down the reaction mixture to room temperature, 48% aqueous NaOH (7.1 g, 0.085 mol) was added to neutralize the HBr. The resulting solution was extracted with ethyl acetate (20 mL ×2), and the organic layer was washed with aqueous NaCl (10 wt%, 20 mL). The solvent was removed under reduced pressure to give the target compound **1**. The crude product was re-crystallized from toluene (8 mL) to give optical pure compound **1** (>99% ee, 2.4 g, 0.015 mol, yield 89%).

Procedure for determination of % ee of **1**:

Compound **1** (0.1 g) was converted to methyl ester by refluxing in HCl in methanol (2 mL) for 12 h. The methyl ester of **1** was analyzed by gas chromatography [column: CHIRASIL-DX CB (25 m, I.D. 0.25 mm, 0.25 μm)].

2.2. Mass spectra and relative vapor pressures

The relative vapor pressures of TFMLA samples as a function of enantiomeric composition were determined by a mass spectrometric approach. The advantage is that volatile impurities are unlikely to contribute to the same fragment mass as TFMLA. On the other hand, both enantiomers of TFMLA have exactly the same mass spectrum and are therefore detected with the same efficiency. The mass spectrometer signal is thus proportional to the sum of the (*R*) and (*S*) partial pressures. By ensuring that the mass flow into the spectrometer is much smaller than the resupply from the solid sample by sublimation, results close to the thermodynamic limit were obtained. Evaporating molecules thus had multiple contacts with racemic and enantiomerically pure crystals before escaping to the spectrometer.

A quadrupole mass spectrometer (Stanford Research Systems RGA 200) was used. Its vacuum chamber was pumped by a small turbomolecular pump (Leybold Turbovac 50) backed by a rotary vane pump (Vacuubrand RS-4) with a cold trap. The samples were thermostatted at 20 °C in a bath cryostat (Haake CH/F3). The vapor was introduced into the mass spectrometer through a high precision needle valve (HOKE Milli-Mite). For a certain setting of the valve a stable dynamical equilibrium of leakage into the chamber and pumping-off was obtained after an induction period of a few minutes. The currents of characteristic fragment ions obtained at an electron impact (EI) energy of 70 eV and measured with a Faraday cup detector were taken as a measure of relative vapor pressure of the parent compound in the sample.

By making sure that the loss through the valve orifice is significantly smaller than the recovery of the gas phase by sublimation, the conducted experiment was close to equilibrium. This was considered essential, because kinetic evaporation effects can easily distort the thermodynamic limit and depend strongly on such aspects as crystal size, morphology, quantity and packing. A drawback of our approach is that the resulting small mass signals do introduce relatively large statistical errors, at this stage of the instrumentation design.

In some experiments, the enantiomerically pure and racemic samples were pumped on for some time prior to measurement to exploit chiroptical self-purification (SDE via sublimation) from traces of the racemic or enantiomerically pure fraction, respectively. A potential disadvantage of this procedure is that it tends to reduce the crystal surface area, like extended storage of the volatile material. This can lead to mass spectrometer loss comparable to the evaporation rate, if insufficient quantities of the compound are used.

All measurements were run for several hours to obtain a stable average value for the intensity of the relevant mass peaks used in Fig. 2. The reproducibility of measurements on different days and the long term drift during one measurement was typically well within 10%. For pressure ratios, this translates into a ≈15% uncertainty, unless several data series are averaged.

2.3. Sublimation pressure diagrams

Important general aspects and quantitative relationships for sublimation phase diagrams shall be explicitly summarized here, because there have been some open issues and ambiguities about them in the literature [1,10,11].

Assume that a compound crystallizes in its enantiomerically pure (*R*) and (*S*) forms, with negligible solubility of the (*R*) compound in the (*S*) crystal and vice versa. The vapor pressure of these crystals is necessarily the same for both enantiomers and will be denoted p_S. Assume further that there is only a single racemic crystal form (*R*/*S*) with its own vapor pressure p_{RS}, again with negligible solubility for (*R*) and (*S*) molecules. For a given temperature *T*, where no liquid state exists for any composition x_R of the (*R*/*S*) mixture, the vapor pressure over a freshly evacuated solid mixture can take either one of three equilibrium values:

(a) p_S, if the solid consists of pure (*S*) or (*R*) crystals,
(b) p_{RS}, if the solid consists of pure (*R*/*S*) crystals,
(c) p_E, the eutectic sublimation pressure, anywhere in between.

For ideal gas behavior and from the Prigogine–Defay equation [26,27], one can derive $p_E/p_S = 1 + (p_{RS}/2p_S)^2$. If the racemate reaches the limiting vapor pressure $2p_S$, it vanishes and the eutectic sublimation pressure is also $2p_S$, as mentioned before. If the racemate is not volatile at all, the eutectic sublimation pressure equals p_S.

For the reverse process of re-sublimation (gas to solid transition) by compression of the gas phase, the first crystals of either (*S*) or (*R*) or (*R*/*S*) will be formed at a range of pressures. Between (*R*) and the eutectic point *ER* in the (*R*)-rich part of the phase diagram, the corresponding pressure is $p = p_R/x_R$ and pure (*R*) crystals will be formed until the eutectic pressure p_E and composition x_E is reached. Beyond p_E there is no gas phase left, somewhat in contrast to a statement in Ref. [1]. Between *ER* and the corresponding eutectic *ES* in the (*S*)-rich part, the pressure is $p = p_{RS}/(2\sqrt{x_R(1-x_R)})$ and racemic crystals will be formed at first. Between the eutectic point in the (*S*)-rich part of the phase diagram, *ES*, and pure (*S*), it is $p = p_S/(1-x_R)$ and pure (*S*) crystals will be formed. These curves are shown in Fig. 1.

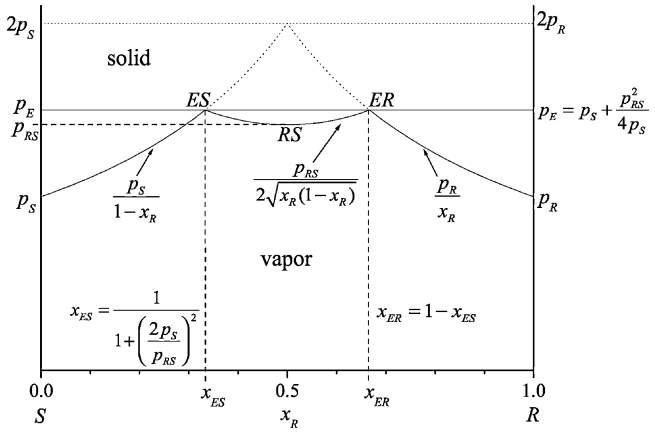

Fig. 1. General sublimation phase diagram for mixtures of a chiral compound (*R*) and its enantiomer (*S*) as a function of composition x_R including a racemic crystal (*R*/*S*) which is more volatile than the enantiomerically pure crystals. See text for explanations. The vapor pressure *p* is plotted relative to that of a pure enantiomer $p_S(=p_R)$. The dotted lines mark the limit of a conglomerate.

The eutectic composition follows from the crossing of the resublimation curves: $x_{ES} = 1/(1 + (2\,p_S/\,p_{RS})^2)$ and $x_{ER} = 1 - x_{ES}$. As a consequence, sublimation will always lead to SDE, unless the starting composition is exactly at an eutectic point (or already in an enantiomerically pure or racemic state). The solid residual material will become enantiomerically pure if the starting composition falls between the pure compound and the closest eutectic and if sublimation is carried out long enough. It will become racemic if the initial composition is between the two eutectic points *ES* and *ER*. Racemate-free conglomerates will always lead to enantiomerically pure residues by sublimation, unless they start with an exact racemic composition. The yield of the enantiomerically pure compound in such a purification process depends on the initial purity in all cases. It will be particularly low in a one-step sublimation process close to an eutectic point.

We establish the sublimation phase diagram by a method which allows for consistency checks. The relative vapor pressure of (*R*) [or (*S*)] and (*R*/*S*) is determined by mass spectrometry. Relative vapor pressure measurements for any intermediate composition are carried out to obtain the eutectic pressure p_E relative to that of the corresponding pure enantiomers p_S.

One should note that racemate and enantiomerically pure crystals will normally have significantly different heats of sublimation. Therefore, the ratio $p_R/\,p_{RS}$ will change with temperature and as a consequence the sublimation eutectics x_{ES} and x_{ER} are also temperature dependent. In particular, they are not necessarily equal to the melting eutectics of the mixture [1]. Because the liquid vaporization enthalpy often does not depend strongly on the enantiomeric purity of the compound [28], the melting and sublimation eutectics may typically fall relatively close together near the temperature of melting [1]. However, exceptions are to be expected [19] and the popular correlation between melting point and volatility [11] should be viewed as a rule, only.

If the (*R*/*S*) form has a smaller enthalpy of sublimation than the (*R*) form, the useful composition range for chiroptical purification of an optically enriched compound may be somewhat increased by lowering the sublimation temperature. However, the speed of sublimation is decreased at the same time. Nevertheless an industrial large-scale application to improve the enantiomeric purity of semi-volatile compounds may be conceived based on this phenomenon. It is a variant of freeze-drying. The ultimate composition range is achieved if the (*R*/*S*) compound reaches twice the vapor pressure of the enantiomerically pure compound. Beyond that value, it will be thermodynamically unstable with respect to a conglomerate [29]. Somewhat opposite arguments apply if the sublimate is used instead of the residue, but in that case, one cannot improve the enantiomeric purity beyond the eutectic composition when working in the thermodynamic limit.

The unusual aspect of TFMLA is that its racemate is about 38 ± 15% more volatile than the enantiomerically pure compound at 20 °C in the thermodynamic limit, as this work will show based on relative vapor pressure determination. Thus, the effects are relatively pronounced, but otherwise entirely general within the constraints formulated at the beginning of this section. Furthermore, the high volatility helps in ensuring solid-solid equilibration, whereas for low volatility compounds like amino acids, metastable mixtures may have to be postulated in some cases [2,20]. E.g., if a stable racemate is produced by mixing equimolar amounts of non-volatile (*R*) and (*S*) crystals, it may take considerable time for the exergonic solid state transformation to complete. In TFMLA, the sublimation/recrystallization pathway can be much faster.

2.4. FTIR spectra

For the pulsed jet FTIR measurements a heated double $10 \times 0.5\ mm^2$ slit nozzle was used to generate cold (about 20 K rotational temperature) clusters of TFMLA. Descriptions of the experimental setup may be found elsewhere [30,31]. In short, gas pulses of 0.3 s duration emerging from the nozzle were synchronized to Fourier transformed infrared (FTIR) scans (Bruker IFS 66v) and the signal was detected by an InSb or HgCdTe detector after optical filtering of unwanted spectral ranges. The intense gas pulses (He with a trace of the acid) were diluted in a large vacuum chamber before being pumped away. The gas mixture was prepared by flowing the He through a heated sample container enclosed between two check valves. The sample container was filled with the enantiomerically pure or racemic compound and dried molecular sieve to keep a large surface and to allow for heating it above the melting point.

For the ATR spectra a single reflection ZnSe ATR unit was used to obtain solid state spectra of finely ground solid TFMLA of different enantiomeric purity. Only spectral regions with significant differences between enantiomerically pure and racemic samples were considered.

2.5. Quantum chemical calculations

Quantum chemical calculations at the B3LYP level with the standard 6-311+G* basis set were performed using the Gaussian 03 program suite [32] for the geometry optimization and frequency calculation of monomers and dimers. To be sure that dispersion effects are unimportant, several structure optimizations were repeated at MP2/6-311+G* level.

Where the experimental dimer bands are compared with the theoretical predictions in figures, all calculated wave numbers are multiplied by a factor to match the experimental monomer transitions. In this way, electronic structure deficiencies and anharmonic contributions to the fundamental vibrations are approximately corrected for, which makes the graphical comparison of dimer band positions more straightforward. Tabulated wave numbers are always unscaled.

3. Results and discussion

3.1. Vapor pressure differences as a function of enantiomeric purity

Relative vapor pressures of the pure (*S*) enantiomer, the racemate and different mixtures of racemate and (*S*) enantiomer

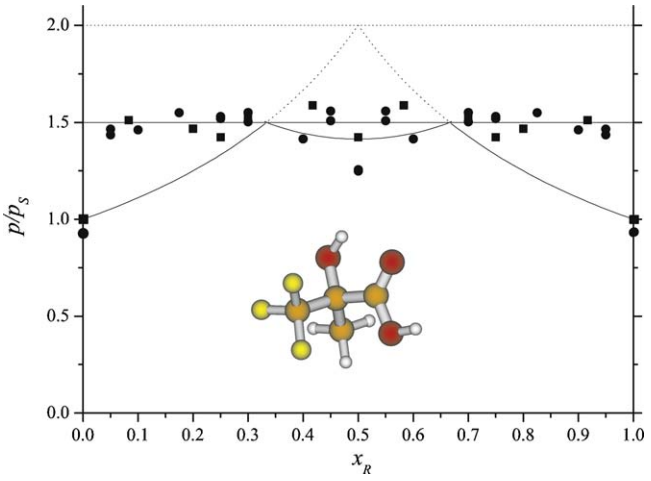

Fig. 2. Vapor pressure diagram of TFMLA measured by mass spectrometry of different mixtures of the (*S*) enantiomer and the racemate. Two independently synthesized batches (circles: batch 1, squares: batch 2) were investigated. The right half of the diagram was completed by symmetry. Mass peaks 63 and 113 were taken into account. The vapor pressures *p* are given relative to the expected value of the pure (*S*) enantiomer p_S, which follows from $p_E/\,p_S = 1.5$.

were determined by mass spectrometry from two batches of the compound (Fig. 2, circles in batch 1 and squares in batch 2). The mass fragments $m = 113$ u (TFMLA–COOH) and 63 u (TFMLA–COOH–CF_2) were used. The vapor pressures shown in Fig. 2 are relative values for the different batches. The right half of the phase diagram was complemented by symmetry. The vapor pressure of the racemate was observed to be $38 \pm 15\%$ higher than that of the pure enantiomer (35% in batch 1 and 42% in batch 2). The vapor pressure of the eutectic is already observed when a small amount of racemate is added to the pure enantiomer or a small amount of pure enantiomer is added to the racemate. Its measured average value was found to be $55 \pm 10\%$ higher (60% in batch 1 and 50% in batch 2) than that of the enantiomerically pure compound in a series of measurements. This result overlaps with the expected value of $48 \pm 10\%$ based on p_{RS} and the crossing point of the two phase coexistence curves in Fig. 1, but the agreement is not perfect in the case of the measurement series denoted by circles. In Fig. 2, we thus plot the phase diagram for the compromise values of $p_{RS}/p_S = \sqrt{2}$ and $p_E/p_S = 1.5$, which are also close to the results from the measurement series denoted by squares (batch 2).

From the measured $(R/S)/(S)$ pressure ratio of 1.38, the position of the eutectic points is predicted at $x_{ES} = 0.32 \pm 0.05$ and $x_{ER} = 0.68 \pm 0.05$. The corresponding critical enantiomeric excess amounts to $35 \pm 10\%$. The compromise choice leads to an enantiomeric excess of 33%. Therefore we can predict that any optically active TFMLA mixture exceeding this approximate ee value will undergo chiroptical self-purification upon room temperature sublimation, if a thick layer of the solid compound ensures equilibration of the solid and vapor phases.

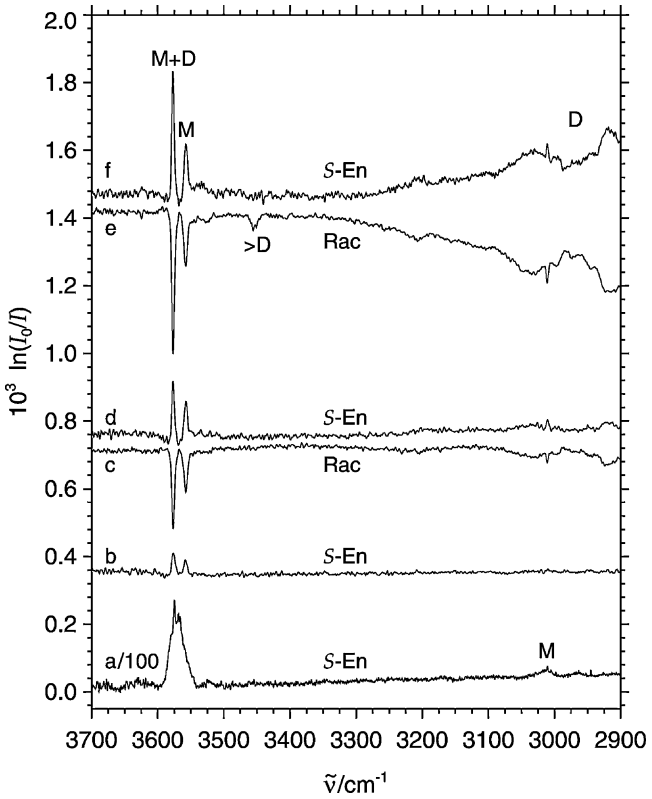

Fig. 3. FTIR spectra in the O–H stretching region: (a) gas phase of the (*S*) enantiomer at room temperature, (b) jet spectrum of the (*S*) enantiomer at low concentration, 880 coadded spectra, (c) jet spectrum of the racemate at medium concentration, 680 coadded spectra, (d) jet spectrum of the (*S*) enantiomer at medium concentration, 480 coadded spectra, (e) jet spectrum of the racemate at high concentration, 640 coadded spectra and (f) jet spectrum of the (*S*) enantiomer at high concentration, 260 coadded spectra. All racemate spectra are inverted for better comparison to the enantiomerically pure compound.

3.2. FTIR spectra

3.2.1. Gas phase and jet FTIR spectra

In the search for a molecular explanation for the unusual volatility of the racemic crystals of TFMLA, molecular dimers play a double role. They are the only realistic candidates for deviations from the ideal gas behavior and they are the smallest supramolecular building blocks towards the crystal.

Room temperature gas phase FTIR spectra were recorded for the racemate and the (*S*) enantiomer in the region from 4000 to 500 cm^{-1}. Due to the low vapor pressure, no bands of aggregates were observed. As a consequence, which is consistent with the high purity of the samples, there were no differences between the spectra for the (*S*) enantiomer and the racemate. Fig. 3 (lowest trace) concentrates on the O–H stretching fundamentals. The bands of the two O–H groups in the monomer (M, see insert in Fig. 2 for the structure) have similar wave numbers. Their rotational contours at room temperature overlap, giving rise to a single broad band. Weak bands near 3000 cm^{-1} are due to monomer C–H stretching fundamentals.

First attempts to expand the room temperature vapor in a supersonic slit nozzle of 600 mm length [33] failed due to the limited volatility. Expansion in a heated nozzle (see Section 2.4) at temperatures between 323 and 363 K resulted in the jet spectra shown in Figs. 3–5. Fig. 3 shows jet spectra of the (*S*) enantiomer and the racemate at different concentrations, controlled by the temperature of the nozzle and of the molecular sieve container. The bands for the two O–H stretching vibrations of the monomer are now well separated in the jet spectra (trace b, most diluted expansion), the band positions are listed in Table 1.

By increasing the concentration, dimer absorptions appear (traces c and d). One would expect two strongly IR active O–H fundamentals for the dimer:

The O–H stretching vibration of the carboxylic O–H group in a dimer is substantially red shifted because of its involvement in a strong intermolecular hydrogen bond. Like in the jet spectra of other carboxylic acid dimers this band is extremely broad and overlaps with the C–H stretching region [34]. It is seen as a baseline oscillation below 3300 cm^{-1}, the sharp peak being due to a superimposed C–H stretching fundamental. No significant differences between enantiomerically pure and racemic expansions (traces d and c) may be seen.

The O–H stretching vibration of the alcoholic O–H-group is expected to be blue shifted in the dimer, because its intramolecular hydrogen bond to the carbonyl group is weakened by the competing intermolecular hydrogen bond of the carbonyl group with a carboxyl O–H of the other molecule. However, no strong new band appears in traces c and d when compared to trace b.

The solution is provided by the spectra recorded at the highest concentration, traces e and f. Here, one can see that the highest frequency monomer band has gained more in intensity than the second highest. Obviously, it is exactly superimposed by the missing dimer O–H stretching band. This also provides a tentative assignment of the two monomer bands. Because of the expected

Table 1
Experimental band positions of the O–H ($>2000\,cm^{-1}$) and C=O ($<2000\,cm^{-1}$) stretching vibrations in the jet FTIR spectra of TFMLA monomers (M), dimers (D) and larger clusters >D. Cluster shifts $\Delta\tilde{\nu}$ (D-M) relative to monomers are also listed.

M/D	$\tilde{\nu}$/cm^{-1}	$\Delta\tilde{\nu}$ (D-M)/cm^{-1}
M + D	3577	+19
M	3558	
>D	3453	−105
D	2900 ± 400	−650 ± 400
M	1783	
D	1732	−51

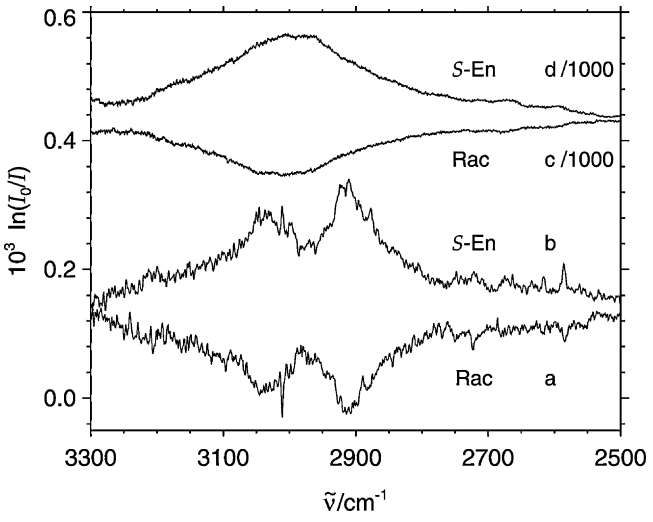

Fig. 4. FTIR spectra in the region of the O–H stretching vibration of the carboxyl group: (a) jet dimer spectrum of the racemate at high concentration, 200 coadded spectra, (b) jet dimer spectrum of the (*S*) enantiomer at high concentration, 320 coadded spectra, sample temperature 10 K higher to compensate for reduced volatility, (c) ATR spectrum of the racemic crystals, (d) ATR spectrum of the enantiomerically pure crystals. The racemate spectra are inverted for better comparison to the enantiomerically pure compound.

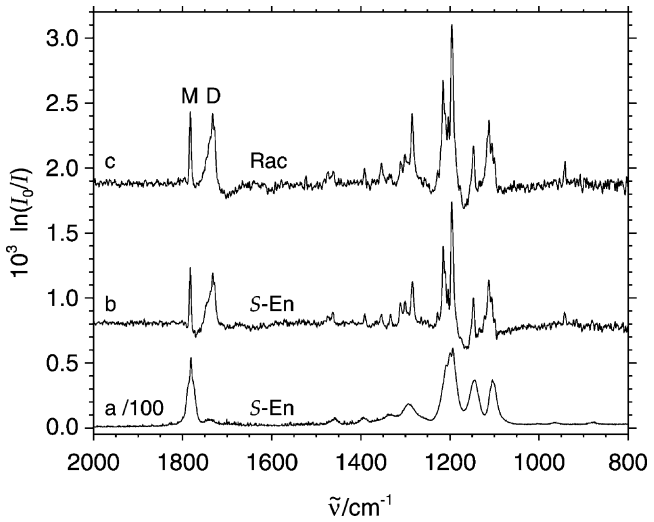

Fig. 5. FTIR spectra in the C=O stretching region: (a) gas phase of the (*S*) enantiomer at room temperature, (b) jet spectrum of the (*S*) enantiomer at 363 K, 560 coadded spectra, (c) jet spectrum of the racemate at 353 K, 320 coadded spectra.

blue shift upon dimerization, it is likely that the weaker and more red-shifted of the two monomer bands is due to the alcoholic O–H group, whereas the stronger band is due to the carboxylic O–H group. Remarkably, the monomer-dimer overlap is perfect in both racemic and enantiomerically pure expansions, pointing at very small chirality recognition effects in the dimers [22]. The alcoholic O–H group of one molecule does not sense the chirality of the binding partner to such an extent that a difference in vibrational frequency results. This is also true for the carboxylic O–H, which is much better defined in traces e and f, but still without any significant spectral difference. A complete picture of the dimer carboxylic stretch is shown in Fig. 4 for the (*S*) enantiomer and the racemate. The slight differences in this region are mostly due to concentration differences and noise. No clearly distinct spectral features due to chirality recognition [22] are observable.

The only significant spectral difference between the two O–H stretching spectra may be found between 3400 and 3500 cm^{-1} in the traces e and f of Fig. 3 recorded at similar concentration. Only the racemic spectrum features a clear peak in this region. An impurity origin has been ruled out by comparing two different sources for the racemate. A dimer origin can be ruled out because the peak is absent in trace c at lower concentration. It must be attributed to a larger cluster, presumably a trimer, involving monomer constituents of different handedness (*S*/*S*/*R*) and (*S*/*R*/*R*).

In the region of the C=O stretching vibration one band is present in the gas phase spectrum and two bands are observed in the jet spectra (Fig. 5). The red shifted band in this region can be attributed to the dimer (D) and possibly to higher clusters as well. Using quantum chemical intensity estimates (vide infra), one can estimate the monomer and dimer concentrations and the dimer fraction in the jet, assuming negligible trimer concentration (Table 2). The absolute and relative numbers are quite comparable for enantiomeric and racemic expansions, although the racemate was recorded at a somewhat lower temperature. This is qualitatively consistent with its higher volatility, which was quantified in the first part of this work. However, it is not reflected significantly in the spectral appearance in the C=O and fingerprint regions shown in Fig. 5, pointing again at negligible chirality recognition at the dimer level.

Undoubtedly, the reason for the vapor pressure differences between the enantiomerically pure and racemic forms must be located in the solid state, not in a different dimer propensity in the gas phase. On the other hand, the higher cluster peak specific to the racemic mixture indicates higher order structural differences, which ultimately lead to the different properties of racemic and enantiomerically pure crystals.

3.2.2. ATR spectra

For further investigations of the crystal state [14], ATR spectra of the racemic and enantiomerically pure crystals have been measured. In both cases, the simple carboxylic acid dimer hydrogen bond C=O···H–O is replaced by cooperative C=O···H–O···H–O sequences, where the central H–O is directly attached to the chirality center of a neighboring molecule (Fig. 6).

This leads to hydrogen bonds of similar strength as in carboxylic acid dimers with similarly broad O–H stretching bands. These are shown in Fig. 4 (top trace). They are rather similar for both crystal forms and close in position to the jet dimer spectra, which also involve twofold coordinated carboxylic O–H groups. In the racemic crystal, two C=O···H–O···H–O hydrogen bond sequences close to a ring, whereas in the enantiomerically pure crystals they are connected with each other in the form of winding chains (Fig. 6). This leads to subtle differences in the IR spectra in various regions (Fig. 7). All bands that show differences between the two spectra in Fig. 7 can be attributed to vibrations involving the O–H groups by comparison to quantum chemical calculations of TFMLA clusters. In the region of 3440–3360 cm^{-1} the O–H stretching vibration of the alcoholic O–H group is observed. It is the solid state analog of the small cluster band marked > D in Fig. 3. The local embedding of this group into the cooperative C=O···H–O···H–O sequence is

Table 2
Number densities and dimer fractions ($c_D/(c_M + c_D)$) determined from the jet FTIR spectra (traces b, c in Fig. 5) in the carbonyl stretching region using reference band strengths from B3LYP/6-311+G* calculations.

Region	M/D	c/cm^{-3}	Dimer fraction
(*S*) enantiomer, 90 °C substance temperature			
C=O	M	4.4×10^{13}	
C=O	D	7.0×10^{13}	0.61
Racemate, 80 °C substance temperature			
C=O	M	5.5×10^{13}	
C=O	D	9.5×10^{13}	0.63

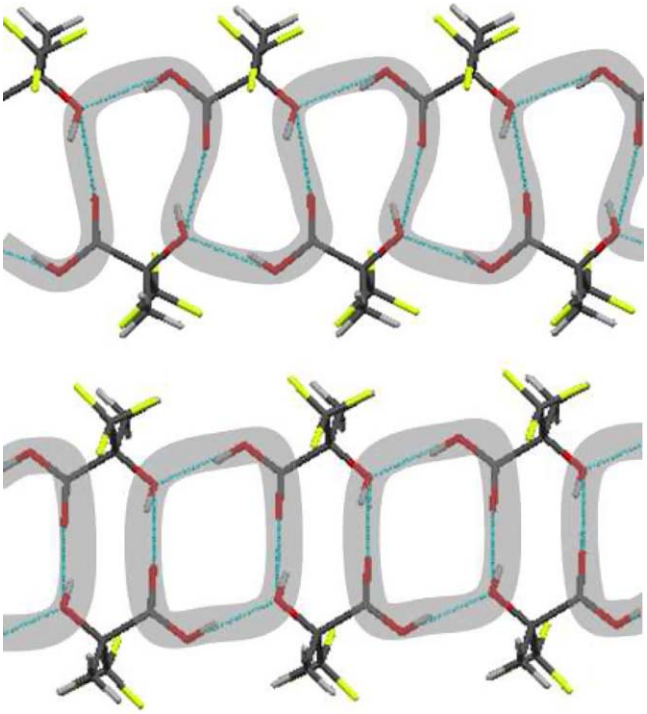

Fig. 6. Sheets of cooperative O–H···O–H···O=C hydrogen bond sequences linked by carboxyl groups in the enantiopure (upper sheet) and the racemic (lower sheet) crystals of TFMLA.

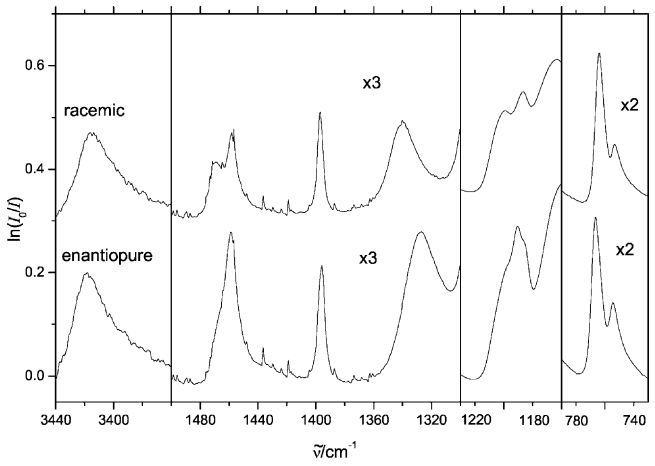

Fig. 7. ATR FTIR spectra of the (*S*) enantiomer (lower spectrum) and the racemate (upper spectrum) in the regions where spectral differences occur.

less perfect in the homochiral winding chains than in the heterochiral enlarged ring [14], thus leading to a reduced red-shift of the O–H stretching vibration by 3 cm^{-1}.

The differences in the other spectral ranges between the racemic and enantiomerically pure forms can also be attributed to the different arrangement and hydrogen bonding network among the racemate and (*S*) enantiomer crystals. The bands shown in the three lower wave number regions in Fig. 7 can be tentatively assigned to vibrations involving in plane bending vibrations of the O–H groups.

Clearly, it is a long way from the simple and chirally non-discriminating dimer hydrogen bond topology to the chirally

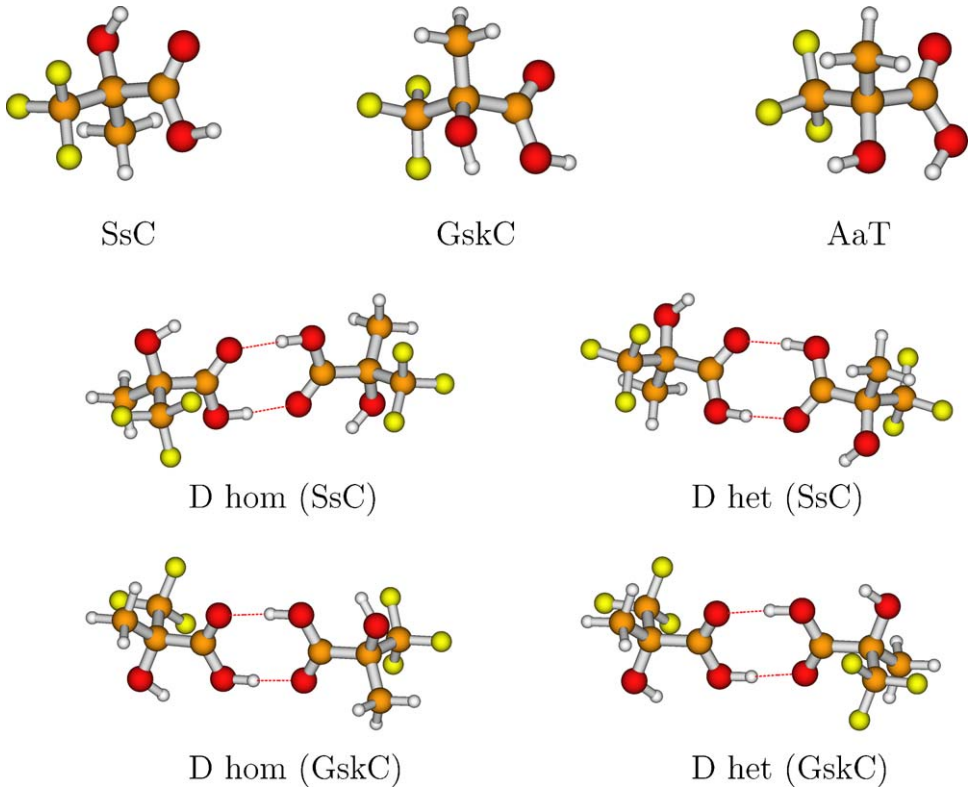

Fig. 8. Most stable monomers and dimers optimized at B3LYP/6-311+G*level. The nomenclature of the conformers describes the torsional angles HO_ACC (syn (S), anti (A) or gauche (G)), $O_ACC{=}O$ (syn (s), skew (sk) or anti (a)) and $O{=}CO_CH$ (cis (C) or trans (T)), the subscripts denote if the oxygen atom is part of the alcoholic hydroxy group (A) or of the carboxyl group (C).

Table 3
Energy differences between monomer conformers without (ΔE_e) and with zero point energy correction (ΔE_0) and dissociation energies of dimers into two SsC monomers without (D_e) and with zero point energy correction (D_0). For the GskC dimers dissociation energies into two GskC monomers are given in parentheses. Results from MP2/6-311+G* geometry optimizations are given in square brackets. Calculated wave numbers (ω/cm^{-1}) and IR band strengths (I/km mol^{-1}) are listed for the O–H and C=O stretching vibrations at B3LYP/6-311+G* level.

B3LYP/6-311+G* [MP2/6-311+G*]						
	ΔE_e/kJ mol^{-1}	ΔE_0/kJ mol^{-1}	ω (O–H)/cm^{-1}	I/km mol^{-1}	ω (C=O)/cm^{-1}	I/km mol^{-1}
SsC			3714	60	1809	323
			3707	70		
GskC	6.3	5.8	3765	48	1835	285
	[5.3]	[5.0]	3729	67		
AaT	11.1	10.4	3785	40	1857	290
			3657	119		
	D_e/kJ mol^{-1}	D_0/kJ mol^{-1}	ω (O–H)/cm^{-1}	I/km mol^{-1}	ω (C=O)/cm^{-1}	I/km mol^{-1}
D_{hom}	62.8	58.3	3722	116	1759	754
(SsC)	[65.7]		3722	1	1710	0
(C_2-Sym.)			3280	2933		
			3204	0		
D_{het}	63.2	59.0	3721	120	1759	752
(SsC)	[66.1]		3721	0	1710	0
(C_i-Sym.)			3283	2953		
			3206	0		
D_{hom}	54.9	50.8	3761	98	1780	671
(GskC)	(67.5)	(62.3)	3760	2	1733	1
(C_2-Sym.)	[58.9]		3246	3200		
	[(69.5)]		3163	1		
D_{het}	55.1	51.5	3758	100	1780	671
(GskC)	(67.8)	(63.0)	3758	0	1734	0
(C_i-Sym.)	[59.1]		3248	3199		
	[(69.7)]		3164	0		

discriminating networks of cooperative C=O···H–O···H–O units involving further interactions to fluorine atoms in the solid state. One can expect that the structure motifs relevant for the crystal will only appear in hydrogen-bonded clusters far beyond the dimers.

3.3. Quantum chemical calculations

To verify the experimental conclusions drawn from the jet spectra, simple quantum-chemical calculations were carried out. Analogously to similar compounds such as lactic acid [35] and α-hydroxy isobutyric acid [36] three monomer conformations were taken into account. Each hydroxy group can act as donor or acceptor for an intramolecular hydrogen bond and an additional acceptor is provided by the carbonyl functionality. The most stable conformer (SsC) involves an intramolecular hydrogen bond from the alcoholic O–H group to the carbonyl group. The second stable GskC conformer has an intramolecular hydrogen bond from the alcoholic O–H group to the carboxylic O–H group and the AaT conformer shows an intramolecular hydrogen bond from the carboxylic O–H group to the alcoholic O–H group. Their optimized structures at B3LYP/6-311+G* level are shown in Fig. 8 and the energy differences are listed in Table 3 together with some MP2/6-311+G* reference calculations. The SsC conformer is by far the most stable monomer and is the only one which is expected and clearly observed in the jet FTIR spectra. The predicted separation of the two O–H stretching bands (7 cm^{-1}) is in only moderate agreement to experiment (19 cm^{-1}), but here we are comparing two rather different electronic environments of the O–H groups, because one is involved in a conjugated COOH system and the other one is engaged in a strained hydrogen bond. Therefore, their close coincidence is the most important and successful prediction. Nevertheless, the lower frequency fundamental is clearly the hydrogen-bonded one according to theory. This agrees with the experimental interpretation given above. Minor quantities of the GskC and AaT conformers were observed in the matrix isolation FTIR spectra of lactic acid and α-hydroxy isobutyric acid. The

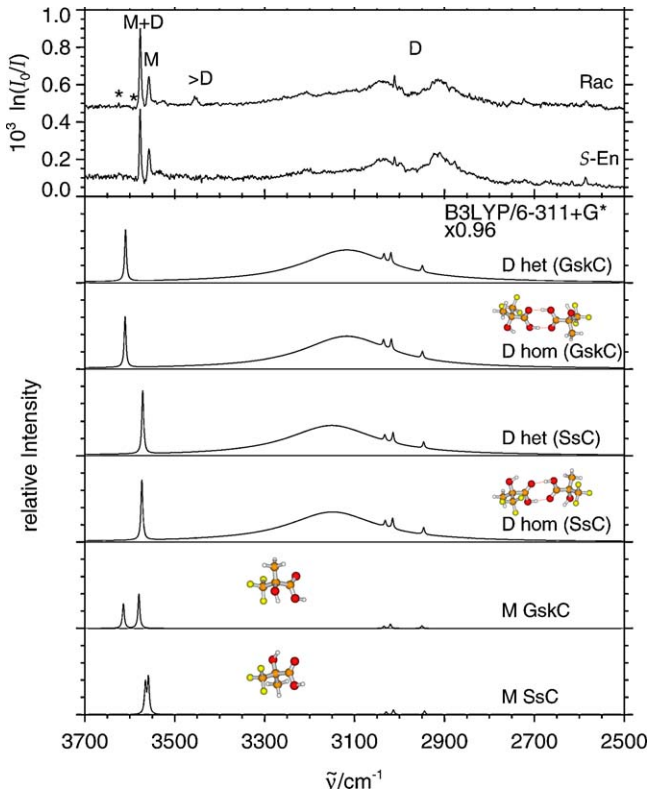

Fig. 9. Jet FTIR spectra of the (*S*) enantiomer (363 K, lower spectrum) and of the racemate (353 K, upper spectrum) in the region of the O–H and C–H stretching vibrations in comparison to the calculated wave numbers for the SsC and GskC monomer and the homo- and heterochiral dimers of both monomer conformations (B3LYP/6-311+G*, scaled by 0.96). The O–H stretching vibration of the carboxyl group in the dimer was simulated by a Lorentzian profile with 250 cm^{-1} full width at half maximum, the other bands with a Lorentzian profile with 5 cm^{-1} full width at half maximum. The GskC contributions are not Boltzmann-weighted because a realistic conformational temperature estimate would render them too small.

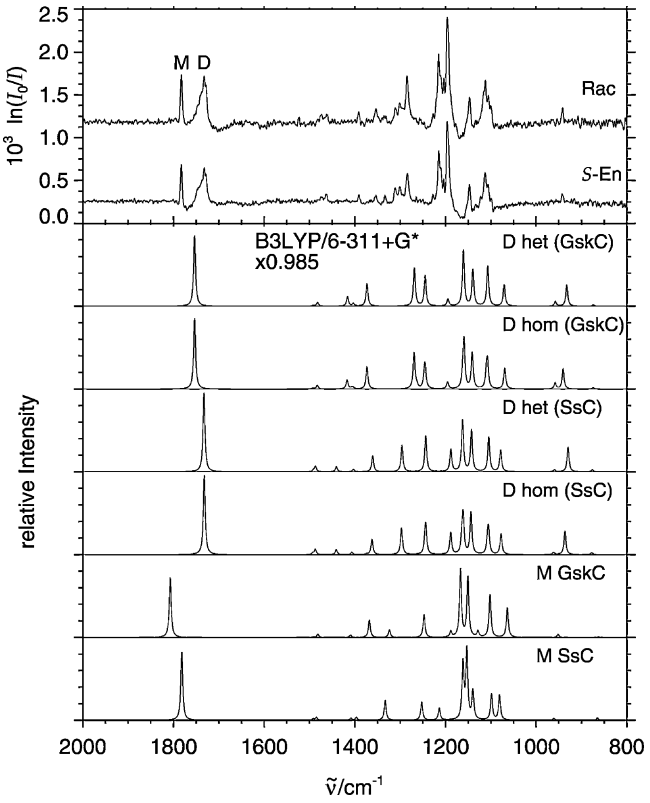

Fig. 10. Jet FTIR spectra of the (*S*) enantiomer (363 K, lower spectrum) and of the racemate (353 K, upper spectrum) in the region of the C=O stretching vibrations in comparison to the calculated wave numbers for the SsC and GskC monomer and the homo- and heterochiral dimers of both monomer conformations (B3LYP/6-311+G*, scaled by 0.985). Dimer intensities are divided by two relative to monomer intensities.

marked bands (*) in Fig. 9 may be due to small fractions of corresponding GskC monomers or possibly dimers of TFMLA.

For the quantum chemical dimer calculations reported here, only the classical carboxylic acid dimer motif with two intermolecular O–H···O=C hydrogen bonds was taken into account because it offers the strongest binding. Other hydrogen bond topologies were tried at low level, but found not to be competitive. Although the energy difference between the SsC and the GskC monomer is rather large, both conformers were considered for the dimer formation. In the dimer formed by two SsC monomers the intra- and intermolecular hydrogen bonds compete for the carbonyl acceptor, whereas in a dimer consisting of two GskC monomers the intra- and intermolecular hydrogen bonds are cooperative. The carboxylic hydroxy group acts as donor and acceptor group at the same time. This cooperativity effect reduces the energy difference between the SsC and GskC dimers compared to that of a pair of monomers (Table 3). However, the effect is not large enough to favor GskC dimers in the jet expansion.

Most relevant for the present work is the chirality discrimination effect [22], namely the energy difference between homochiral and heterochiral SsC dimers. It is seen to be very small, less than 1 kJ/mol or 2%. In line with this, the predicted spectral differences between the two dimers are very minor, almost within numerical accuracy. This is not surprising, because the carboxylic acid dimer structure keeps the chirality centers far apart. Hydroxy esters, in contrast, allow for a much closer approach of the chirality centers and lead to more pronounced effects [37]. Hence, the experimental lack of chirality discrimination at the dimer level finds qualitative and quantitative confirmation in the calculations.

Fig. 9 shows the comparison of the calculated wave numbers and the experimental spectra in the high frequency range. Different half-widths are used to qualitatively mimic the extended Fermi resonance pattern of the carboxylic hydrogen bonds, on which weak C–H fundamentals are superimposed. The red-shift of the carboxylic O–H bands is somewhat underestimated, as usual. The near-coincidence of the higher frequency monomer and dimer O–H fundamentals is qualitatively reproduced. As expected, basically all spectral features in the jet spectra can be explained with the most stable SsC monomer and the most stable homo- and heterochiral SsC dimers. The feature marked >D requires an explanation beyond the dimer.

Fig. 10 shows the corresponding simulations in the C=O and fingerprint regions. Again, there is no reason to invoke a contribution from the GskC isomer. The homo- and heterochiral dimer fundamental vibrations agree very closely in both experiment and theoretical prediction. There is one isolated O–H out of plane bending vibration of the carboxylic O–H group near 950 cm^{-1} where they are predicted to differ slightly by about 3 cm^{-1}, but this small difference is not found in the experimental spectrum.

4. Conclusions

Chiral hydroxy acids are known to have a tendency towards unstable racemates, which has been related to the role of the hydroxy group in suppressing centro-symmetric dimer arrangements [38]. This "enantiophobicity" [39] appears to be enhanced by fluorination. Indeed, the racemate of TFMLA is considerably more volatile than the enantiomerically pure crystals. The present study has derived the approximate sublimation phase diagram of this compound below room temperature and it has provided infrared spectra of the isolated dimers under supersonic jet conditions.

The relative vapor pressure as a function of enantiomeric composition was found to be consistent with immiscibility in the solid state and pure monomer evaporation. TFMLA represents a pronounced case of racemate volatility, which leads to chiroptical self-purification by thermodynamically controlled sublimation at ee-values above ≈33%.

No chirality recognition was observed in the carboxylic acid dimers. The most stable dimers show two O–H···O=C hydrogen bonds which separate the chirality centers. Chirality recognition effects are thus restricted to larger clusters and the bulk solid phase. In contrast, the related ester methyl lactate already shows chirality recognition effects in dimers, trimers and tetramers [22,37,40]. This may be explained by the lack of a rigidly planar supramolecular recognition unit [23], allowing the chiral parts of the molecules to approach each other more closely to result in chiral recognition.

It will be interesting to extend the present phase diagram to lower temperature to see whether the eutectic composition changes. This requires improvements of the mass spectrometry setup, which would also help to narrow down the error margins of the present investigation. The study of sublimation under kinetic control and the extension to even more extreme cases of chirality dependent evaporation phenomena [19] will be of interest. Spectroscopically, it will be instructive to study the corresponding esters, which allow for a more intimate contact of the asymmetric centers in dimers.

Acknowledgements

The present work was supported by the Fonds der Chemischen Industrie and by the DFG research training group 782 (www.pcgg.de). J. Zischang and B. Kovacikova have contributed

importantly to this study during research internships. U. Schmitt has designed the mass spectrometer setup for relative vapor pressures.

References

[1] J. Jacques, A. Collet, S.H. Wilen, Enantiomers, Racemates, and Resolutions, John Wiley and Sons, 1981.
[2] P. Cintas, Angew. Chem. Int. Ed. 47 (2008) 2918–2920.
[3] T. Ushio, R. Tamura, H. Takahashi, N. Azuma, K. Yamamoto, Angew. Chem. Int. Ed. Engl. 35 (1996) 2372–2374.
[4] Y. Hayashi, M. Matsuzawa, J. Yamaguchi, S. Yonehara, Y. Matsumoto, M. Shoji, D. Hashizume, H. Koshino, Angew. Chem. Int. Ed. 45 (2006) 4593–4597.
[5] R. Breslow, M.S. Levine, Proc. Natl. Acad. Sci. U.S.A. 103 (2006) 12979–12980.
[6] P. Diter, S. Taudien, O. Samuel, H.B. Kagan, J. Org. Chem. 59 (1994) 370–373.
[7] V.A. Soloshonok, D.O. Berbasov, Chim. Oggi/Chem. Today 24 (2004) 44–47.
[8] V. Nieminen, D.Y. Murzin, K.D. Klika, Org. Biomol. Chem. 7 (2009) 537–542.
[9] G. Pracejus, Liebigs Ann. Chem. 622 (1959) 10–22.
[10] H. Kwart, D.P. Hoster, J. Org. Chem. 32 (1967) 1867–1870.
[11] D.L. Garin, F.J. Cooke Greco, L. Kelly, J. Org. Chem. 42 (1977) 1249–1251.
[12] R.H. Perry, C. Wu, M. Nefliu, R.G. Cooks, Chem. Commun. (2007) 1071–1073.
[13] S.P. Fletcher, R.B.C. Jagt, B.L. Feringa, Chem. Commun. (2007) 2578–2580.
[14] V.A. Soloshonok, H. Ueki, M. Yasumoto, S. Mekala, J.S. Hirschi, D.A. Singleton, J. Am. Chem. Soc. 129 (2007) 12112–12113.
[15] R. Kuroda, S.F. Mason, J. Chem. Soc., Dalton Trans. (1979) 273–278.
[16] Y. Mastai, A. Völkel, H. Cölfen, J. Am. Chem. Soc. 130 (2008) 2426–2427.
[17] F. Nerdel, W. Diepers, Tetrahedron Lett. 18 (1962) 783–786.
[18] B. Koppenhoefer, U. Trettin, Fresenius Z. Anal. Chem. 333 (1989) 750.
[19] T. Katagiri, C. Yoda, K. Furuhashi, K. Ueki, T. Kubota, Chem. Lett. 25 (1996) 115–116.
[20] D.G. Blackmond, M. Klussmann, Chem. Commun. (2007) 3990–3996.
[21] G.L. Perlovich, S.V. Kurkov, L.K. Hansen, A. Bauer-Brandl, J. Pharm. Sci. 93 (2004) 654–666.
[22] A. Zehnacker, M.A. Suhm, Angew. Chem. Int. Ed. 47 (2008) 6970–6992.
[23] Z. Xue, M.A. Suhm, J. Chem. Phys. 131 (2009) 054301.
[24] Z. Su, N. Borho, Y. Xu, J. Am. Chem. Soc. 128 (2006) 17126–17131.
[25] G.M. Florio, E.L. Sibert III, T.S. Zwier, Faraday Discuss. 118 (2001) 315–330.
[26] I. Prigogine, R. Defay, Chemische Thermodynamik, VEB, Leipzig, 1962.
[27] M. Farina, J. Incl. Phenom. Mol. Recognit. Chem. 14 (1992) 101–111.
[28] J. Groh, Ber. Dtsch. Chem. Ges 45 (1912) 1441–1447.
[29] J.S. Chickos, D.L. Garin, M. Hitt, G. Schilling, Tetrahedron 37 (1981) 2255–2259.
[30] C. Cézard, C.A. Rice, M.A. Suhm, J. Phys. Chem. A 110 (2006) 9839–9848.
[31] M. Albrecht, C.A. Rice, M.A. Suhm, J. Phys. Chem. A 112 (2008) 7530–7542.
[32] M.J. Frisch, G.W. Trucks, H.B. Schlegel, G.E. Scuseria, M.A. Robb, J.R. Cheeseman, J.A. Montgomery Jr., T. Vreven, K.N. Kudin, J.C. Burant, J.M. Millam, S.S. Iyengar, J. Tomasi, V. Barone, B. Mennucci, M. Cossi, G. Scalmani, N. Rega, G.A. Petersson, H. Nakatsuji, M. Hada, M. Ehara, K. Toyota, R. Fukuda, J. Hasegawa, M. Ishida, T. Nakajima, Y. Honda, O. Kitao, H. Nakai, M. Klene, X. Li, J.E. Knox, H.P. Hratchian, J.B. Cross, C. Adamo, J. Jaramillo, R. Gomperts, R.E. Stratmann, O. Yazyev, A.J. Austin, R. Cammi, C. Pomelli, J.W. Ochterski, P.Y. Ayala, K. Morokuma, G.A. Voth, P. Salvador, J.J. Dannenberg, V.G. Zakrzewski, S. Dapprich, A.D. Daniels, M.C. Strain, O. Farkas, D.K. Malick, A.D. Rabuck, K. Raghavachari, J.B. Foresman, J.V. Ortiz, Q. Cui, A.G. Baboul, S. Clifford, J. Cioslowski, B.B. Stefanov, G. Liu, A. Liashenko, P. Piskorz, I. Komaromi, R.L. Martin, D.J. Fox, T. Keith, M.A. Al-Laham, C.Y. Peng, A. Nanayakkara, M. Challacombe, P.M.W. Gill, B. Johnson, W. Chen, M.W. Wong, C. Gonzalez, J.A. Pople, Gaussian 03, Revisions B.04 and C.02, Gaussian Inc., Pittsburgh PA, 2003.
[33] N. Borho, M.A. Suhm, K. Le Barbu-Debus, A. Zehnacker, Phys. Chem. Chem. Phys. 8 (2006) 4449–4460.
[34] T. Häber, U. Schmitt, C. Emmeluth, M.A. Suhm, Faraday Discuss. 118 (2001) 331–359.
[35] A. Borba, A. Gómez-Zavaglia, L. Lapinski, R. Fausto, Phys. Chem. Chem. Phys. 6 (2004) 2101–2108.
[36] S. Jarmelo, R. Fausto, Phys. Chem. Chem. Phys. 4 (2002) 1555–1563.
[37] N. Borho, M.A. Suhm, Org. Biomol. Chem. 1 (2003) 4351–4358.
[38] M. Simonyi (Ed.), Problems and Wonders of Chiral Molecules, Akademiai Kiado, Budapest, 1990.
[39] L. Pérez-García, D.B. Amabilino, Chem. Soc. Rev. 36 (2007) 941–967.
[40] T.B. Adler, N. Borho, M. Reiher, M.A. Suhm, Angew. Chem. Int. Ed. 45 (2006) 3440–3445.